Research Article

Chemical weathering intensity and rare earth elements release from a chlorite schist profile in a humid tropical area, Bengbis, Southern Cameroon

Vincent Laurent Onana[a*], Estelle Ndome Effoudou[b], Sylvie Desirée Noa Tang[b], Véronique Kamgang Kabeyene[b], Georges Emmanuel Ekodeck[a]

[a]Department of Earth Sciences, Faculty of Science, University of Yaoundé I, P.O. Box 812, Yaoundé, Cameroon. Corresponding author: onana.vl@gmail.com Tel.: +237 6 77 75 94 21

[b]Department of Geology, Higher Teacher Training College, University of Yaoundé I, P.O. Box 47, Yaoundé, Cameroon.

Résumé

Un profil d'altération développé sur chloritoschistes de la zone de Bengbis (Sud Cameroun) a été choisi pour quantifier l'intensité de l'altération et comprendre le comportement des terres rares. Les valeurs de l'indice d'altération mafique combinées aux diagrammes ternaires du système Al – Fe – Mg – Ca – Na – K montrent que l'hydrolyse des feldspaths est proportionnelle à celle des minéraux mafiques (pertes en Mg), bien que l'hydrolyse des plagioclases (Ca, Na) soit plus intense que celle des minéraux ferromagnésiens. Les matériaux d'altération étudiés sont localisés dans le domaine de la kaolinitisation, à l'exception des matériaux nodulaires qui sont légèrement latritiss. La modification du comportement du Mg dans le milieu d'altération s'exprime par les faibles valeurs du rapport Ca/Mg. Le potassium et Be sont lessivés dans le sol en association avec Mg. L'ordre de mobilité des éléments dans l'environnement d'altération étudié est : Ca ≈Na > Fe^{2+} ≈Sr > Mg ≈ Co > Mn > Li > Ba > Rb > P > Cd > Ni > Si > Be > K > Sn. Les enrichissements en K, Cs et Be dans les saprolites sont liés à la présence d'illite. L'accumulation en Cs dans le sol est due à la présence de kaolinite. Le système le plus stable dans le milieu d'altération étudié est : Hf – Nb – W – U. Les saprolites, les matériaux nodulaires et les matériaux argileux meubles superficiels sont appauvris en terres rares par rapport à la roche mère. Les terres rares présentent trois types de comportement le long du profil d'altération, comme l'indiquent les valeurs du rapport $(La/Yb)_N$ ($(La/Yb)_N < 1$, $(La/Yb)_N \sim 1$ et $(La/Yb)_N > 1$). Les terres rares légères et les terres rares moyennes s'accumulent dans les matériaux d'altération pour des valeurs de pH comprises entre 5,5 et 5,6 et pour celles de Eh variant entre +60 et +70mV. L'ordre de mobilité de ces éléments dans ces matériaux est le suivant : terres rares moyennes > terres rares lourdes ≈ terres rares légères. Ce fait est contre-intuitif, car les terres lourdes sont plus mobiles dans les environnemenst supergènes que les terres rares légères. L'adsorption ou la co-précipitation de ces terres rares sur les oxydes de fer peut principalement contrôler la concentration de ces éléments dans le profil d'altération. Les faibles anomalies en Ce dans les matériaux d'altération de la zone de Bengbis, dues au changement de Ce^{3+} en Ce^{4+}, sont probablement dues à la présence de faibles quantités de rhabdophane. Les matériaux d'altération étudiés présentent un fractionnement en Gd ($Gd/Gd^* \sim 0.70 – 0.84$) dues à une intense lixiviation. Ce fait a rarement été signalé dans un environnement d'altération latéritique. Il semble qu'une partie de la distribution et de la remobilisation du gadolinium soit contrôlée par des minéraux mafiques dans les matériaux d'altération étudiés. La distribution et la mobilisation des terres rares sont donc contrôlées par (1) l'adsorption ou la co-précipitation dans les minéraux mafiques et Fe, (2) et légèrement par les minéraux contenant des terres rares tels que le rhabdophane, rencontrés dans les matériaux d'altération étudiés.

Mots clés : Chloritoschistes; Latérites; Indices chimiques d'altération; anomalie en Ce; Afrique centrale

Received: 23/09/2020

Accepted: 13/10/2020

DOI: https//dx.doi.org/10.4314/jcas.v16i2.5

Abstract

An *in situ* weathering profile overlying chlorite schists in southern Cameroon was chosen to quantify chemical weathering intensity and to study the behaviour of rare earth elements (REE). Mafic index alteration values combined with the ternary diagrams of the Al – Fe – Mg – Ca – Na – K system show that the hydrolysis of feldspars is proportional to that of mafic minerals (losses in Mg), although the hydrolysis of the plagioclases (Ca, Na) is more intense than that of ferromagnesian minerals. The studied materials are localised in the domain of kaolinitisation, except for nodular materials which are slightly lateritised. The change in the behaviour of Mg in the weathering environment is expressed by the low values in Ca/Mg ratio. Potassium and Be are leached in the soil in association with Mg. The order of mobility of the elements in the weathering environment is: Ca ≈Na > Fe^{2+} ≈Sr > Mg ≈Co > Mn > Li > Ba > Rb > P > Cd > Ni > Si > Be > K > Sn. The enrichments in K, Cs and Be in saprolites are linked to the presence of illite. Cesium accumulation in the soil is due to the presence of kaolinite. The most stable system is: Hf – Nb – W – U. Saprolites, nodular and loose clayey materials are depleted in REE relative to the parent rock. REE exhibit three types of behaviour along the Bengbis profile like indicated by $(La/Yb)_N$ ratio values ($(La/Yb)_N < 1$, $(La/Yb)_N \sim 1$ and $(La/Yb)_N > 1$). Light REE and Middle REE accumulate in the weathering materials for pH values ranging between 5.5 and 5.6 and for those of Eh varying between +60 and +70mV. The order of mobility of REE in these horizons is: Middle REE > Heavy REE ≈ Light REE. This fact is counter-intuitive, because Heavy REE are more mobile in supergene environment than Light REE. Adsorption or co-precipitation of LREE onto Fe oxides mainly may control the concentration of these elements in the profile. Weak Ce anomalies in the weathering materials of Bengbis area, due to the change in Ce^{3+} to Ce^{4+}, are probably due to the presence of low amounts in rhabdophane. The studied weathering materials show a fractionation in Gd ($Gd/Gd^* \sim 0.70 – 0.84$) due to intense chemical leaching. This fact has been rarely reported in lateritic weathering environment. It appears that, a part of Gd distribution and remobilization is controlled by mafic minerals in the studied weathered materials. REE distribution and mobilization are thus controlled by (1) adsorption or co-precipitation in mafic and Fe minerals, (2) and slightly by REE-bearing minerals such as rhabdophane found in the studied weathering profile.

Keywords: Chorite schists; Laterites; Chemical weathering indices; Ce anomaly; Central Africa

1. Introduction

Lateritic materials are heterogeneous due the nature of the parent rock, climate, biology (vegetation and fauna) and topography (Tardy, 1993). This heterogeneity makes the understanding of the mechanisms of their genesis and their supergene evolution relatively complex. This led scientists to use diverse approaches, mineralogical, thermodynamic and kinetic, mass balance and restructuring methods to quantify processes that take place during weathering. Apart from mass balance and restructuring methods, numerous chemical weathering indices are also used in the geochemical approach. However, these indices have many limitations. For example, the use of chemical index of alteration (CIA) of Nesbitt and Young (1982, 1984, and 1989) presents the disadvantage of not taking into consideration the redox dependent behaviour of iron. In addition, CIA is inefficient in the study of most advanced weathering materials. New weathering indices (Mafic index of alteration (MIA) and, Index of lateritisation (IOL)) by Babechuk et al. (2014) enable the quantification of the behaviour of mafic minerals in the study of rock weathering processes. Moreover, it has been shown that, the knowledge of the behaviour of trace elements, especially rare earth elements (REE), gives useful information on the oxidation state in the weathering environment (Braun et al., 1993; Ndjigui et al., 2008; Kamgang et al., 2009; Nyassa Ohandja et al., 2020). Relevant studies have been carried out on the weathering and the behaviour of these REE on granito-gneissic (Zheng and Lin, 1996; Nesbitt and Markovics, 1997; Bao and Zhao, 2008), volcanic (Irfan, 1999; Patino et al., 2003; Babechuk et al., 2014), carbonate (Walter et al., 1995; Bourbon et al., 2009), and metamorphic rocks (Gardner and Walsh, 1996; Kamgang et al., 2009; Rajamani et al., 2009; Gong et al., 2011). These scientific works have shown that the distribution and mobilization of REE are (1) mainly controlled by minerals such as monazite, allanite, xenotime, zircon, rhabdophane, and clay minerals, (2) and that the only two REE that may show signs of anomalous behaviour are Ce and Eu, depending on the oxidizing or reducing conditions prevailing in the weathering environment. The aim of this study is to quantify the intensity of supergene weathering, using weathering indices that take into account the hydrolysis of mafic minerals, and explain gadolinium anomalies in relation to the different stages of chlorite schists weathering along lateritic profiles, wherein the distribution and mobilization of REE is not controlled by clay minerals but mainly by mafic minerals and iron oxyhydroxides.

2. Location, Geology and Climate

The Mbalmayo-Bengbis series, roughly limited between 2° and 4° North and 11° and 16° East, occupies the central part of the Cameroonian Southern Plateau and belongs to the Yaounde Group. Metapelites and meta-psammopelites of the Yaounde Group underwent a multiphase deformation history which can be subdivided into the stages D_1-D_2, D_3 and D_4 (Owona et al., 2010). The deformation stage D_1-D_2 has a progressive character and led to the formation of the regionally dominant foliation S_2 (Owona et al., 2010). The Bengbis region, located in these geological formations has been selected as study site (Fig. 1). The parent rock is a greenish, shiny at the surface and foliated chlorite schist. Millimetre-size concordant quartz veins within the chlorite schist are observable, although chlorite schists in this region are more alkaline than those of Mbalmayo (Kamgang et al., 2009). Also, the greenish colour is due to a high amount of chlorite contained in the Bengbis rocks. Microtectonic study shows that the phenomenon of mylonitisation is pronounced in the Bengbis rocks (Onana, 2010). Quartz, muscovite, chlorite, plagioclases and opaque minerals are smaller in size than those observed in chlorite schists of the

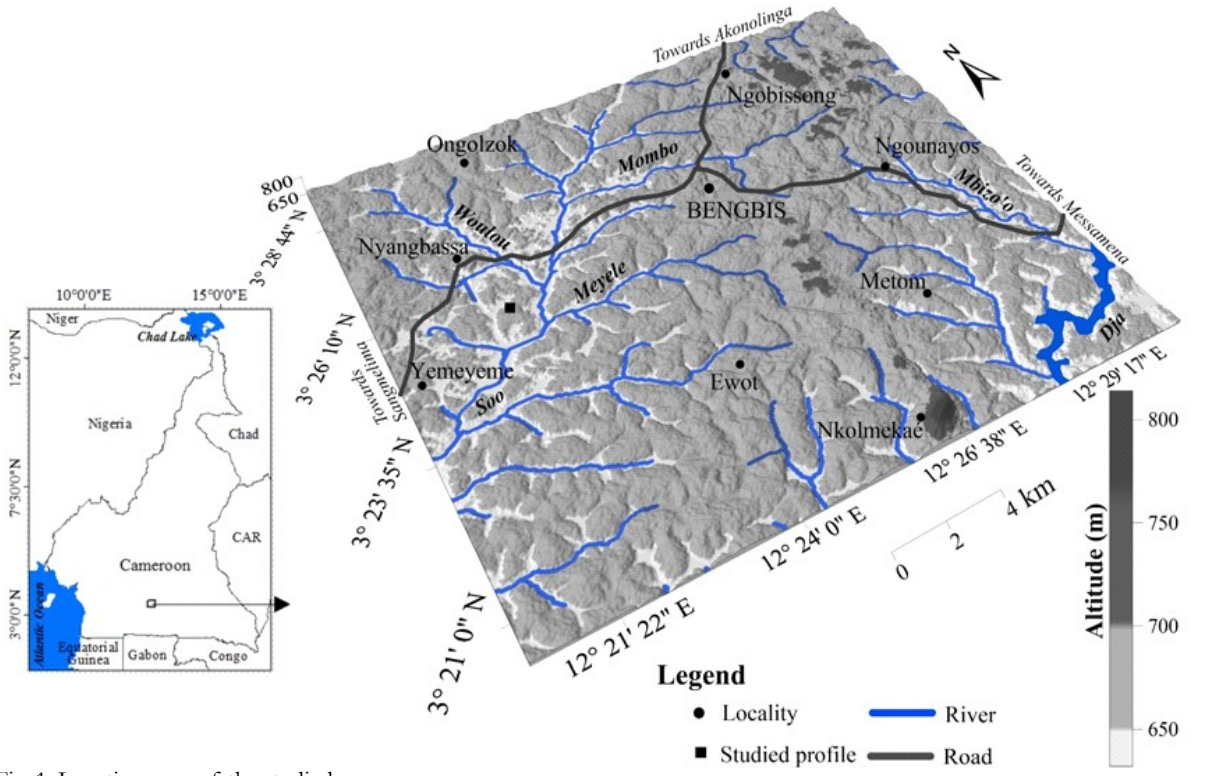

Fig. 1. Location map of the studied area

Mbalmayo region (Kamgang et al., 2009). These rocks generate low plateaus (600–700 m) (Santoir, 1995). A landscape of hills close to large valleys is observed. The total annual rainfall is 1668 mm and the average annual temperature is 24.2°C (Suchel and Tsalefac, 1995). The actual climate is of equatorial type with transition nuance of oceanic traits.

3. Materials and methods

On the Nyangbassa asymmetrical interfluves, located within the most representative morphological unit (Fig. 1), the thickness of the weathering profile is about 16 m on the top (Pit BE3). Only the pit at the top of the interfluve, showing the sharpest lateral and vertical pedological variations, was studied in detail. After a macroscopic description of the profiles (after Duchaufour, 1977), 14 samples were collected from each horizon of the profile for physical, mineralogical, and chemical analyses. Undisturbed samples were collected for density measurements. Bulk density values were determined by Flint and Flint's method (Flint and Flint, 2002). The mineralogical composition of the rocks and the weathering cover was determined by X-ray diffraction on the total fine fractions.

The samples were then analysed by XRD using Co radiation at 40 kV and 45 mA at the Geoscience Laboratories (GeoLabs) of the Ontario Geological Survey in Sudbury Ontario (Canada). Major element concentrations were determined by X-ray fluorescence after sample ignition. Sample powders were ignited and then melted with lithium tetraborate flux before analysis using a Rigaku RIX-3000 wavelength-dispersive X-ray fluorescence spectrometer. Rock powders were prepared for inductively coupled plasma mass spectrometry analysis (ICP-MS) for trace element concentrations by acid digestion in closed beakers. Rock powders were dissolved in a mixture of HCl and $HClO_4$ acids at 120°C in sealed teflon containers for 1 week. The containers were rinsed with diluted HNO_3 and the solutions boiled to dryness. The residue was dissolved in HCl and $HClO_4$ and evaporated to dryness a

second time, before being dissolved again in a mixture of HNO_3, HCl and HF at 100°C. Ferrous iron concentrations were obtained by potassium dichromate titration. Sample solutions were analysed in a Perkin-Elmer 5000 ICP-MS instrument. At first the analysis was performed using the IM100 analytical package, in which a weighted average of instrument responses for three certified reference materials prepared in the same manner as the unknown was compared with the instrument response of the unknown solution for each element.

The nominal zero concentration was assumed to be equal to the measured response from an acid blank. Standard solutions were run between each batch of 30 samples along with a check sample for every 14 samples. Data are reported for 14 rare earth elements (La, Ce, Pr, Nd, Sm, Eu, Gd, Tb, Dy, Ho, Er, Tm, Yb, and Lu). The pH and Eh of soils samples were determined with the aid of a Shott Gerate CG818 pH-Eh meter. Their colour was obtained using a Munsell soil colour chart (Munsell Color, 2000). The formulae of weathering indices proxy used are:

$$CIA = 100 \times [Al_2O_3/(Al_2O_3 + CaO^* + Na_2O + K_2O)] \quad (1)$$

A value of 100 indicates complete removal of the mobile elements. The molar CaO is corrected for the presence of carbonate and apatite as for the CIA (e.g., Fedo et al., 1995) to consider only the silicate-bound Ca (CaO*).

In oxidising environment and when Fe is retained, total Fe is considered an immobile element along with Al (Al_2O_3) and the MIA calculation is:

$$MIA_{(O)} = 100 \times [(Al_2O_3 + Fe_2O_{3(t)})/(Al_2O_3 + Fe_2O_{3(t)} + MgO + CaO^* + Na_2O + K_2O)] \quad (2)$$

$MIA_{(O)}$ increasing index values represent progressively more altered rock, as it is the case with the CIA. A value of 100 indicates complete removal of the mobile elements.

The index of lateritisation IOL uses the mass (wt.%) ratio of SiO_2, $Fe_2O_{3(t)}$, and Al_2O_3. The IOL calculation is:

$$IOL = 100 \times [(Al_2O_3 + Fe_2O_{3(t)})/(SiO_2 + Al_2O_3 + Fe_2O_{3(t)})] \quad (3)$$

Unweathered mafic rocks have IOL values that are less than 40. In the same manner as CIA and MIA, higher IOL values correspond to more intensely weathered materials (Babechuk et al., 2014).

4. Results, Interpretation and Discussion

4.1. Macroscopic and mineralogical description of weathered materials

The lateritic weathering profile of Bengbis is located at the summit of an interfluve, under a secondary Equatorial forest at 695 m of altitude. It has a total thickness of 16 m and presents from bottom to top, a saprolitic zone, a nodular level and a loose sandy clayey zone (Fig. 2).

The saprolitic zone has a thickness greater than 12 m. It is divided into two main horizons, which are from bottom to top, the coarse saprolite and the fine saprolite.

The coarse saprolite whose thickness is higher than 11 m with an average bulk density of 1.3 g/cm^3, presents five facies of different colours from the bottom: friable yellow (10YR 8/8) facies with compact blocs, compact red (10R 7/8) facies, friable yellow (10YR 8/8) facies and reddish (10R 7/6) facies overlaid by yellow (10YR 8/6) material.

The friable coarse saprolite (4.60 m) is a clayey material with a well-preserved parent rock structure. This clay embeds compact blocs where primary minerals are visible (quartz and phyllites).

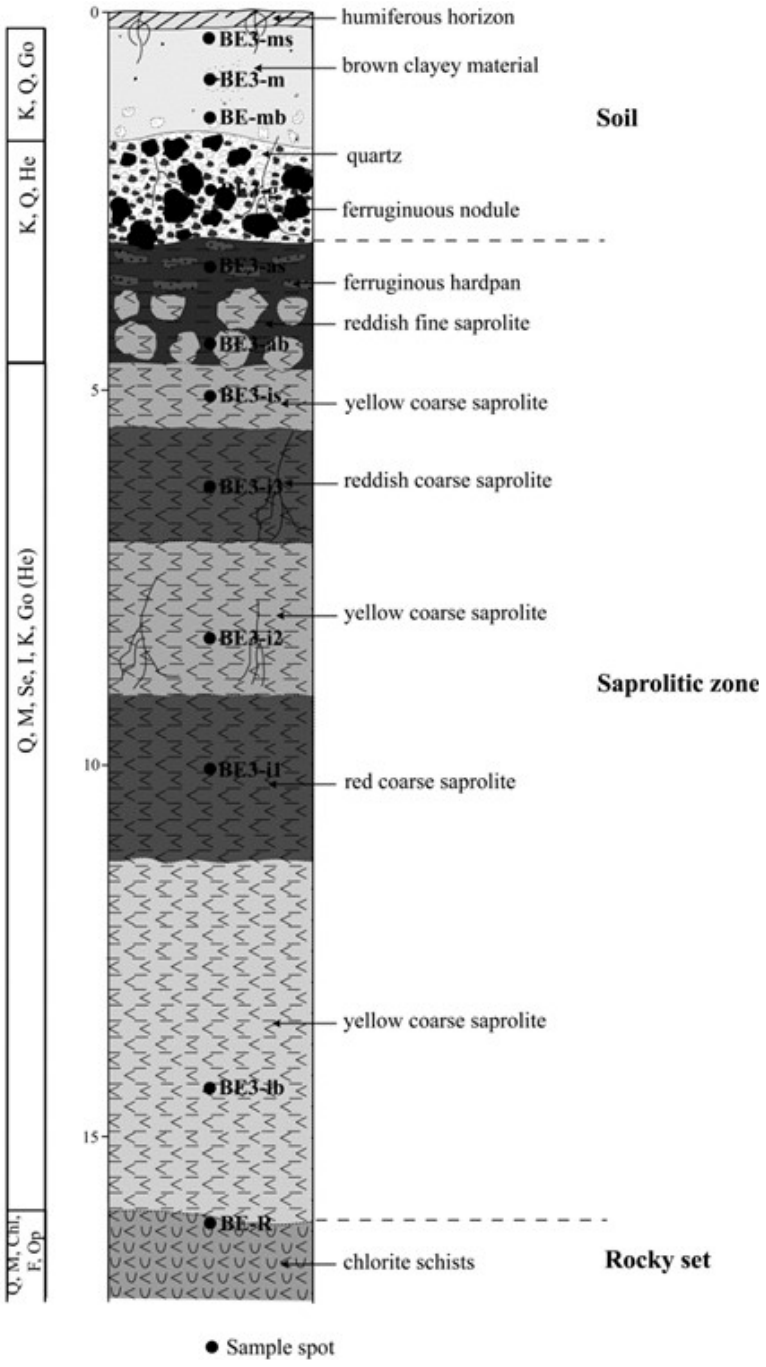

Fig. 2.Geological sketch section of the Bengbis lateritic profile

Phyllosilicates are soft and black in colour. They are already affected by the weathering. The passage to the overlying facies is diffuse.

The red coarse saprolite (2.40 m) is a sandy clayey material with a banded structure. Visible minerals are quartz and relics of phyllosilicates. The transition between this purplish to red material and the yellow facies is gradual.

The yellow coarse saprolite (2 m) is a clayey friable material. The structure of the parent rock is quite visible. The recognisable mineral is quartz.

The reddish coarse saprolite (1.45 m) is a silty clayey, friable and dense material. Recognisable minerals are quartz which constitutes light bands and, phyllites such as muscovite, abundant in the

dark bands. Dark bands are more abundant than the quartzo-feldspathics ones.

The yellow coarse saprolite presents the same characteristics with the underlying facies except that it is less thick (0.90 m). The transition of this coarse saprolite with the overlying fine saprolite is sharp.

The fine saprolite (1.55 m) is a reddish (10R 6/6) clayey material, friable, porous and less dense (da = 1.3 g/cm^3). This reddish clay which represents almost 50% of the material encloses pluri-centimetric indurated fragments. These red fragments present in their edges, a yellow clayey fine film and their nucleus is bright red. This set is reminiscent of a carapace. Inside this yellow matrice, there are also centimetre-sized scales whitish grey rock fragments with well-preserved chlorite schist structure. These scales for which mineralogical transformations preserve the characteristics of fine saprolite, without creating new structures are alloteritic hardpans (Boulangé, 1984). Transition to the nodular level is progressive.

With 1.40 m in thickness and a bulk density of 1.4 g/cm^3, the medium level is a red (10R 4/8) clayey material (~50%) containing blocks of various nature (quarzitic and ferruginous) and sizes as well as centimetre-sized nodules. Blocks are observed preferentially at the top of the nodular level. Two types can be described, (1) blocks of quartz, which represent at most 5% of this part of the profile, (2) ferruginous blocks whose dimensions vary between 15 cm x 9.5 cm and 28 cm x 28 cm, and whose proportion reaches 10%. These blocks co-exist with the ferruginous nodules constituting almost 35% of the materials. The quantity of these nodules decreases towards the summit. Many roots of trees with sizes close to 8 cm in diameter are also visible. Transition to the uppermost part is sharp.

The loose superficial level (1.70 m) is a brown (7.5YR 5/4) clayey material, very porous (da = 1.3 g/cm^3) and friable. It is dotted with many roots and rootlets and is made up in its first thirty centimetres by a humus rich A horizon. The weathered materials are distinguished by (1) the high thickness of the alterites and the low soils thickness, and (2) the presence of an alloteritic carapace at the top and bottom of the slope in comparison with those of Mbalmayo (Kamgang et al., 2009; Onana et al., 2016). The coarse saprolite is made up of quartz, muscovite, illite-smectites, sericite, kaolinite and goethite (Table 1). The alloteritic hardpan is made up of quartz, muscovite, kaolinite, goethite and hematite. Interstratified illite-smectites disappeared from the mineral assemblage at the top the fine saprolite. Minerals present in the nodular horizon are hematite, kaolinite, quartz and goethite. The nodules and the matrix contain the same minerals. Quartz, kaolinite and goethite are the main minerals present in the loose clayey set. Nevertheless, traces of hematite still remain at the base of this part. The mineralogical composition of the weathered materials is identical to that of Mbalmayo region (Kamgang et al., 2009; Onana et al., 2016) and those developed on sericite-quartz schists in China (Gong et al., 2011).

4.2. Major, trace elements and quantification of the extent of weathering

The average CIA value for mica schists is 63.5 according to the USGS standard (Smith, 1998). Like these rocks, chlorite schists present values of CIA of 62.9. These CIA values are lower than those of the chlorite schists (CIA = 50.8) in the Mbalmayo region (Kamgang et al., 2009). This difference might be because chlorite schists of Bengbis area and those of Mbalmayo, both alkaline (Numbem et al., 2007) present some differences in their mineralogical composition. Calcite is present in the chlorite schists of Bengbis, which are richer in chlorite.

Vertical distribution of major elements along the profile (Table 1; Fig. 3) shows five types of major elements behaviour. In general, Al_2O_3 and P_2O_5 have the same saw-toothed evolution along the profile.

Table 1. Mineralogical, pH – Eh, major (wt. %) and trace element (ppm) data for the Bengbis chlorite schist profile

	Rocky set	Saprolitic zone						Soil					
	Chlorite schist	Coarse saprolite					Fine saprolite	Nodular horizon			Loose sandy clayey horizon		
Code	BE-R	BE3-ib	BE3-il	BE3-i2	BE3-i3	BE3-is	BE3-ab	BE3-as	BE3-g	BE3-gn	BE3-gm	BE3-mb	BE3-m	BE3-ms
Depth (m)	16.00	14.40	9.40	8.40	6.20	5.15	4.50	3.55	2.40	2.40	2.40	1.60	0.85	0.25
pH	7.16	5.59	5.65	5.54	5.41	5.47	4.78	5.00	5.70	-	-	4.80	5.59	5.75
Eh (mV)	-31.1	+61.1	+58.8	+64.6	+72.6	+68.6	+109.6	+96.6	+92.4	-	-	+108.3	+62.0	+52.5
Mineralogy	Q M Chl F Op	Q M Se I K Go	Q M Se I K Go	Q M Se I K Go	Q M Se I K Go	Q M Se I K Go	Q M Se K I-Sm Go	Q M K I-Sm Go	Q K He	Q K He	Q K He	Q Se K Go	Q Se K Go	Q K Go
SiO_2	*0.01**	64.62	68.83	60.68	60.88	61.71	47.85	51.75	32.02	19.12	46.70	67.09	68.68	73.51
Al_2O_3	*0.01*	14.14	13.60	18.97	18.94	16.22	21.41	21.82	16.82	15.16	19.67	13.35	13.73	11.05
MgO	*0.01*	2.01	0.97	1.15	1.02	1.02	0.93	1.00	0.32	0.10	0.54	0.41	0.43	0.34
MnO	*0.01*	0.08	0.03	0.03	0.04	0.03	0.07	0.11	0.03	0.01	0.02	0.03	0.03	0.03
CaO	*0.01*	0.77	0.00	0.01	0.04	0.00	0.00	0.04	0.04	0.00	0.04	0.02	0.05	0.02
Na_2O	*0.01*	2.78	0.07	0.07	0.09	0.06	0.06	0.06	0.03	0.00	0.05	0.00	0.02	0.03
K_2O	*0.01*	2.60	3.93	4.57	3.76	4.01	2.75	2.84	0.62	0.29	1.20	0.75	0.88	0.69
Fe_2O_3	*0.01*	5.40	7.90	7.71	8.38	10.53	14.83	11.16	38.48	51.91	8.59	9.03	6.98	5.08
FeO	*0.01*	3.91	0.29	1.18	0.87	0.99	0.52	0.42	0.00	0.00	0.26	0.20	0.37	0.51
TiO_2	*0.01*	0.84	1.02	0.97	1.09	0.97	1.01	1.19	0.93	0.83	0.85	0.98	1.27	1.14
P_2O_5	*0.01*	0.19	0.05	0.20	0.12	0.27	0.25	0.12	0.11	0.11	0.05	0.04	0.07	0.05
LOI	*0.05*	5.88	3.52	5.52	6.16	5.44	10.76	9.98	10.89	12.31	22.27	8.25	8.16	8.04
Total	-	*99.31*	*99.92*	*99.89*	*100.32*	*100.27*	*99.92*	*100.08*	*100.29*	*99.87*	*99.97*	*99.96*	*100.30*	*99.98*
CIA	-	63	85	76	80	83	81	90	88	97	100	94	95	94	94
$MIA_{(O)}$	-	57	80	74	76	79	78	86	84	97	99	90	91	90	90
IOL	-	23	27	24	31	31	30	43	39	63	78	38	25	23	18
LILE															
Rb	*0.23*	118.42	48.88	105.6	65.31	127.13	79.61	45.56	138.68	52.38	19.78	78.12	66.58	88.48	69.93
Sr	*0.6*	111.40	23.40	15.40	33.90	16.90	25.60	5.00	22.30	10.80	8.50	14.00	10.70	13.90	11.40
Ba	*0.8*	512.62	323.58	485.59	399.17	571.85	523.2	236.88	506.13	155.20	99.87	221.69	128.74	157.31	116.66
Cs	*0.013*	5.78	5.90	8.92	8.68	8.87	7.86	7.25	9.57	3.68	1.46	6.87	5.30	5.92	4.91
Li	*0.4*	46.07	26.80	32.69	37.80	38.53	23.73	30.79	38.12	11.54	4.09	22.26	19.10	20.90	14.80
HFSE															
Nb	*0.028*	15.4	15.1	18.2	18.6	19.2	15.3	21.9	23.7	19.0	16.8	20.6	17.9	20.5	18.4
Hf	*0.14*	6.2	6.2	8.1	6.6	6.5	5.6	6.6	7.2	7.5	7.0	5.3	5.2	5.7	5.6
Th	*0.06*	14.67	12.76	14.15	12.65	13.74	13.28	8.15	16.81	33.78	41.86	15.99	12.07	13.00	10.31
U	*0.007*	2.65	4.05	3.76	4.08	4.24	5.51	5.35	3.33	4.55	5.34	2.88	2.33	2.51	2.13

However, the evolution of Al_2O_3 is opposed to that of SiO_2 (Fig. 3a). CaO, Na_2O and FeO, in major contents in the rock decrease in the weathering materials where they remain as traces, whereas Fe_2O_3

*Detection limit; Q: quartz; M : muscovite; Chl: chlorite; F: feldspar; Op: Opaques; I: illite; I-Sm: I–Sm:															
Zr	*4*	228.1	223.8	288.6	231.7	236.1	198.3	234.6	260.5	255.7	293.0	201.7	186.9	209.8	203.3
W	0.05	1.54	1.64	2.18	2.41	2.14	1.89	2.70	2.42	2.04	1.94	1.88	1.40	1.53	1.26
Mo	*0.08*	0.17	2.87	1.23	2.66	1.22	2.39	3.69	2.94	9.27	6.50	2.86	2.27	2.29	1.88
FeMg element															
Cr	*8*	79.89	77.62	96.92	104.10	109.10	83.12	150.70	160.16	655.70	832.30	88.99	98.45	91.97	63.96
Ni	*0.8*	36.22	51.34	16.25	32.01	29.60	33.03	60.60	32.24	22.47	17.77	29.70	20.48	21.93	17.85
V	*1*	110.00	117.10	156.10	160.20	161.60	130.50	181.80	202.27	584.40	781.50	159.30	123.30	117.30	91.27
Co	*0.1*	15.06	7.80	3.75	5.19	4.42	5.08	8.16	7.80	4.33	4.26	5.40	5.16	5.49	4.83
Sc	*0.60*	15.12	10.08	16.52	9.18	28.21	22.34	22.19	26.92	33.26	43.45	23.43	13.22	15.91	10.98
Other element															
Be	*0.04*	2.68	3.64	3.61	4.41	3.80	3.44	3.24	2.73	1.13	0.95	1.57	0.99	0.91	0.78
Cu	*0.7*	28.95	47.64	24.28	29.31	26.70	46.60	41.24	37.75	79.82	127.60	30.70	28.65	27.37	22.38
Cd	*0.013*	0.07	0.05	0.07	0.06	0.05	0.05	0.06	0.06	0.07	0.08	0.05	0.04	0.06	0.05
Ga	*0.04*	19.62	21.78	25.54	27.08	26.29	23.72	27.95	30.69	37.76	46.10	26.17	18.11	19.42	15.11
Tl	*0.005*	0.70	4334.10	5268.48	5069.65	0.94	4162.69	5181.55	0.98	0.36	4414.91	4696.03	5010.05	0.58	5778.55
La	*0.02*	57.50	213.00	24.14	151.00	16.49	178.00	9.17	49.98	23.00	18.52	26.70	19.67	24.85	17.05
Ce	*0.07*	88.40	441.00	62.44	227.00	40.80	432.00	25.84	116.05	52.82	26.28	85.97	55.15	74.41	43.53
Pr	*0.006*	11.130	39.400	5.283	37.290	4.111	36.720	2.497	10.476	4.187	2.848	5.337	3.958	5.192	3.326
Nd	*0.03*	42.55	106.00	16.89	129.00	14.54	112.00	9.10	34.60	13.50	8.84	17.83	13.36	17.34	11.06
Sm	*0.01*	8.09	15.35	3.17	22.25	2.89	18.75	1.81	5.77	2.42	1.68	2.90	2.33	3.09	1.96
Eu	*0.005*	1.750	2.334	0.596	3.767	0.563	2.959	0.340	1.022	0.466	0.375	0.538	0.426	0.577	0.380
Gd	*0.009*	8.160	5.783	2.313	12.076	1.973	1.973	7.949	3.271	1.758	1.545	1.922	1.474	1.991	1.383
Tb	*0.003*	1.120	0.870	0.410	1.640	0.342	1.100	0.210	0.486	0.320	0.320	0.320	0.260	0.350	0.260
Dy	*0.008*	6.600	4.715	2.722	8.199	2.566	5.473	1.423	3.104	2.255	2.315	2.159	1.856	2.606	1.927
Ho	*0.003*	1.270	0.833	0.572	1.188	0.609	0.873	0.315	0.634	0.504	0.542	0.473	0.410	0.599	0.445
Er	*0.008*	3.260	2.463	1.798	2.947	2.074	2.423	1.023	1.954	1.597	1.755	1.494	1.333	1.962	1.498
Tm	*0.003*	0.420	0.361	0.276	0.390	0.321	0.343	0.160	0.299	0.245	0.269	0.229	0.203	0.294	0.231
Yb	*0.01*	2.52	2.45	1.94	2.48	2.22	2.27	1.09	2.01	1.67	1.80	1.52	1.33	1.89	1.50
Lu	*0.003*	0.350	0.343	0.294	0.314	0.328	0.305	0.161	0.288	0.249	0.272	0.224	0.184	0.269	0.209
ΣREE	-	233.13	834.91	98.70	599.54	89.83	801.17	54.35	229.99	104.99	67.36	147.62	101.95	135.42	84.76
LREE/HREE	-	14.41	72.96	14.72	36.51	9.71	66.52	11.61	26.17	14.71	8.37	22.75	17.77	16.39	13.24
$(La/Yb)_N$	-	2.25	8.55	3.17	5.99	0.73	7.72	0.83	2.45	1.36	1.01	1.73	1.46	1.29	1.12
$(La/Yb)_{chl}$	-	1.00	3.81	1.41	2.67	0.33	3.44	0.37	1.09	0.60	0.45	0.77	0.65	0.58	0.50
Sm/Nd	-	1.00	0.76	0.99	0.91	1.05	0.88	1.05	0.88	0.94	1.00	0.86	0.92	0.94	0.93
Eu/Eu*	-	1.00	1.15	1.02	1.06	1.09	1.12	1.06	1.09	1.05	1.08	1.06	1.07	1.08	1.07
Ce/Ce*	-	1.00	1.38	1.58	0.87	1.42	1.53	1.55	1.45	1.54	1.04	2.06	1.79	1.87	1.65
Gd/Gd*	-	1.00	0.70	0.81	0.84	0.77	0.76	0.79	0.80	0.78	0.77	0.80	0.76	0.76	0.76
Fe^{2+}/Fe^{3+}	-	4.12	0.21	0.04	0.20	0.13	0.12	0.04	0.04	-	-	0.03	0.03	0.06	0.13
Ca/Na		0.28	0.25	0.00	0.14	0.44	0.00	0.00	0.67	1.33	-	0.80	-	2.49	0.67
Ca/Mg	-	0.33	0.02	0.00	0.01	0.03	0.00	0.00	0.03	0.11	0.00	0.06	0.04	0.10	0.05

interstratified illites-smectites; Se: sericite; K: kaolinite; Go: goethite; He: hematite;

$CIA = Al_2O_3 / (Al_2O_3 + CaO^* + Na_2O + K_2O)$; $MIA_{(O)} = 100 \times [(Al_2O_3 + Fe_2O_{3(t)})/(Al_2O_3 + Fe_2O_{3(t)} + MgO + CaO^* + Na_2O + K_2O)]$; $IOL = 100 \times [(Al_2O_3 + Fe_2O_{3(t)})/(SiO_2 + Al_2O_3 + Fe_2O_{3(t)})]$; $(La/Yb)_N = (La/La_N)/(Yb/Yb_N)$; $(La/Yb)_{chl} = (La/La_{chl})/(Yb/Yb_{chl})$; $Eu/Eu^* = (Eu/Eu_{chl})/(Sm/Sm_{chl})^{1/2}(Gd/Gd_{chl})^{1/2}$; $Ce/Ce^* = (Ce/Ce_{chl})/(La/La_{chl})^{1/2}(Pr/Pr_{chl})^{1/2}$; $Gd/Gd^* = (Gd/Gd_{chl})/(Eu/Eu_{chl})^{1/2}(Tb/Tb_{chl})^{1/2}$ – chl: chlorite schist – N: NASC values (After Gromet et al., 1974)

contents increase (Fig. 3b). K_2O and MgO are present in major amounts in the chlorite schist and saprolites and decrease in soil horizons where they occur in minor amounts (Fig. 3c). The lowest K_2O and MgO contents are observed in the nodular materials and nodules. MnO and TiO_2 are relatively stable in the weathering profile (Fig. 3d). These two oxides accumulated extensively in nodular materials.

pH-Eh data indicate that Bengbis weathering materials evolve in an acidic weathering environment while chloriteschists are alkaline reducing materials (Table 1).

Weathered materials of the coarse saprolite have CIA values varying between 76 and 85. This fact indicates a moderate weathering that is consistent with the presence of clays such as illite and illite/smectite mixed layers (Babechuk et al., 2014) in these materials as shown by X-Ray diffraction data (Table 1).

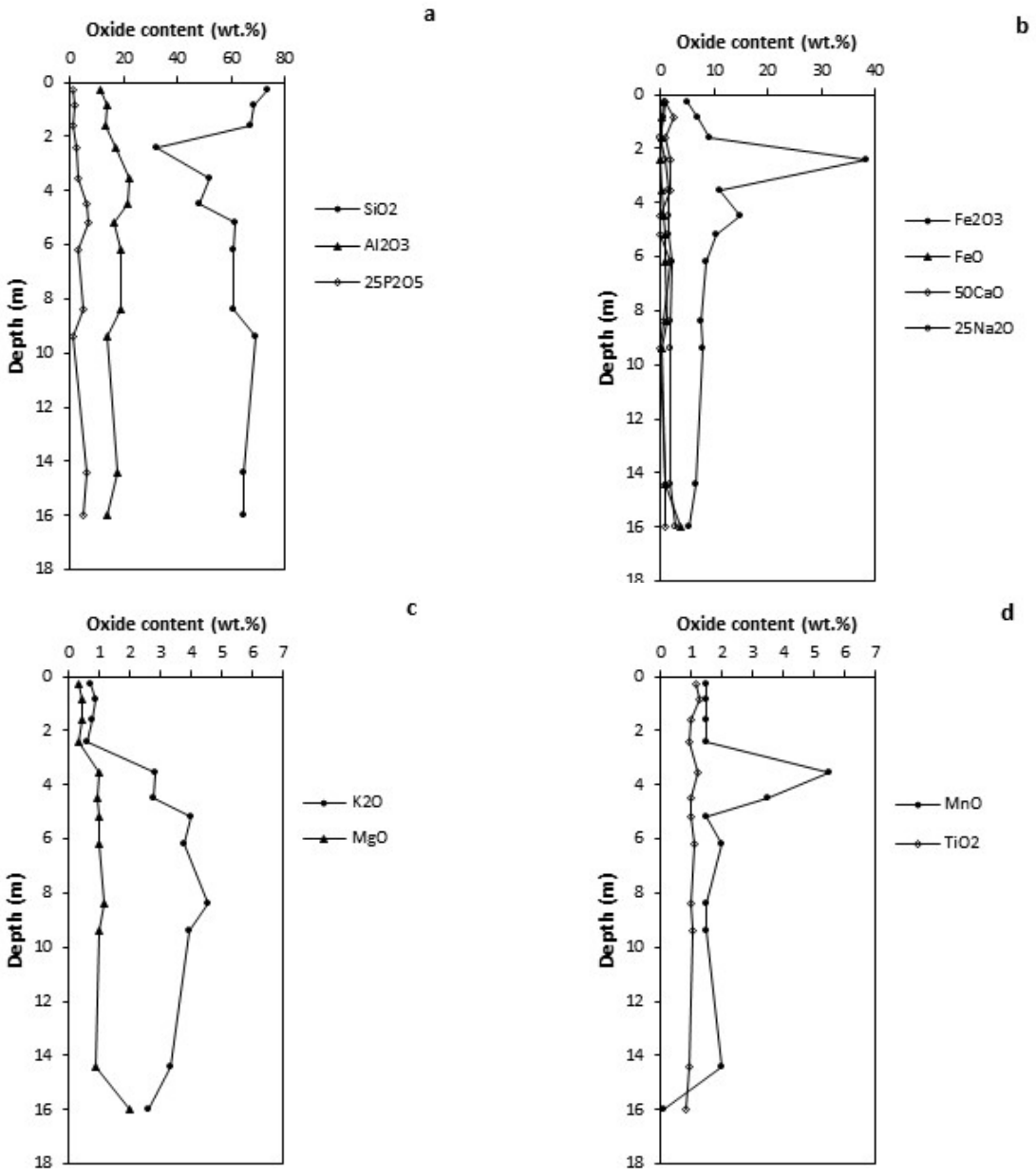

Fig. 3. Major elements (wt.%) distribution along the Bengbis lateritic profile

CIA values range between 88 and 100, from fine saprolite to soils, indicating the total loss of bases. The most weathered materials of the Bengbis region have reached the stage of complete kaolinitisation as indicated by the presence of kaolinite in the studied profile. However, CIA is not appropriate for the quantification of advanced weathering processes. In fact, the predominant hydrolitic process in the meteoric weathering is de-silicification but silicon is not taken into consideration in the CIA calculation (Babechuk et al., 2014). The CIA strength is the utility of the accompanying A–CN–K diagram (Nesbitt and Young, 1984; Nesbitt, 1992). In this diagram (Fig. 4), weathered materials follow a parallel evolution to A–K axis. This corresponds to a total loss of Ca and Na and, reflects the presence of muscovite in relatively significant contents in the weathering environment, except in the nodular horizon (0.62 wt.%), nodules (0.29 wt.%) and in loose sandy clayey materials (0.75 wt. %). Minor K contents (< 0.1 wt.%) in these materials correspond to the disappearance of muscovite in the weathering horizon. The phenomenon is equally observable on the weathering materials overlying alkaline chlorite schists in the Mbalmayo area (Kamgang et al., 2009).

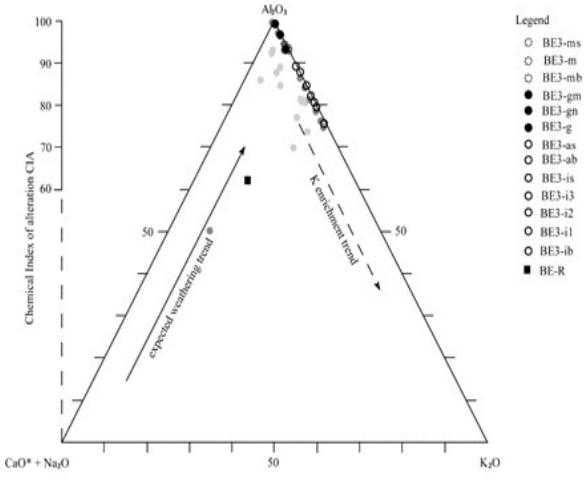

Fig. 4. Molar Al_2O_3–CaO* + Na_2O–K_2O (A–CN–K) ternary plot illustrating the different degrees of alteration in Bengbis profile. Shaded circles are data from Kamgang et al. (2009) and Gong et al. (2011)

Although not localised on the A–K axis like those of Bengbis and Mbalmayo regions, weathering materials on sericite-quartz schists of the Yunnan province in China (Gong et al., 2011) present a similar evolution, enrichment in K, less than 30% (Fig. 4). This fact is different from that observed on the weathered materials overlying basalts in India where laterites show an evolution towards A apex, parallel to A–CN axis and the absence of muscovite (Babechuk et al., 2014). Generally, during the weathering of schistose rocks, for a CIA value of ~70, the dissolution rate of plagioclases (CaO + Na_2O) is ~90%.

MIA values are average, below 60 and relatively close to those of CIA. This relative distance is because the USGS standard used is that of mica schists and not that of chlorite schists. These MIA values are greater than those of the alkaline metabasites of the Mbalmayo region (47.9). Although close, $MIA_{(O)}$ values are slightly inferior to those of CIA. MIA and CIA values are well correlated ($r^2 = 0.99$), confirming the similar global behaviour of Mg, Ca and Na (Babechuk et al., 2014). Generally, CIA and MIA values present an arithmetic progression of reason 4 (CIA = MIA + 4), except for the nodular materials (BE3-g and BE3-gn), probably because of their zero FeO content relative to other materials.

This progress is materialised by a gap between curves representing CIA and MIA (Fig. 5), along the weathering profile, reflecting a minor retention of the Mg in the weathered materials while Ca and Na are abundantly evacuated during feldspar dissolution from the base of the profile. Magnesium might probably be retained in the illite-smectites. This is similar to the observations made on the weathered materials developed over chlorite schists in Mbalmayo region. A gap appears from the base to the summit of curves representing CIA and MIA in the weathered materials overlying sericite-quartz schists of the Yunnan region in China (Gong et al., 2011). In fact, FeO exists in minor quantities (0.1–1 wt.%) in the weathered

materials from the base to the summit of the profiles.

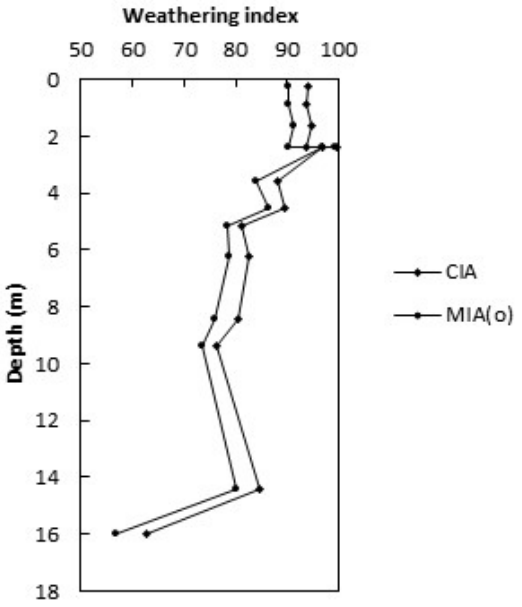

Fig. 5. Stratigraphic variation of the weathering indices ($MIA_{(O)}$ and CIA) along Bengbis profile

Fe^{2+}/Fe^{3+} ratio values decrease from chlorite schists (4.12) to weathered materials (0.03), while CIA and MIA values increase (Table 1). This reflects the conversion of Fe^{2+} into Fe^{3+} with the increase of the weathering and therefore the accumulation of iron (Fe^{3+}) in weathering oxidizing environment into iron oxides. Thus, the new MIA weathering index is more sensitive to certain changes that appear in the weathering profile than CIA.

Associated to MIA, weathering processes can be graphically quantified in the A–Fe–Mg–Ca–Na–K system with the help of two ternary diagrams inspired by Nesbitt and Young (1989), Nesbitt and Wilson (1992) and Babechuk et al. (2014).

The materials of the Bengbis profile are aluminous. The A–L–F diagram (Fig. 6a) shows a significant decrease of labile elements (Mg, Ca, Na, K) in the weathering environment. Lateritisation only affects nodular materials developed over chlorite schists like in Mbalmayo region. It should be noted that this phenomenon is more pronounced at Mbalmayo than Bengbis (Fig. 6a). This behaviour is similar to that of materials developed on basalts of the Bidar region in India (Babechuk et al., 2014). Weathered materials on the Yunnan region (China) are not lateritised (Gong et al., 2011).

The AF–CNK–M diagram (Fig. 6b) shows that the hydrolysis of feldspar (loss in Ca, Na and K) is proportional to those of mafic minerals (loss in Mg), although the weathering of plagioclases (Ca, Na) is more intense than that of mafic minerals (Mg). The same process has been observed in Mbalmayo and at Yunnan (China).

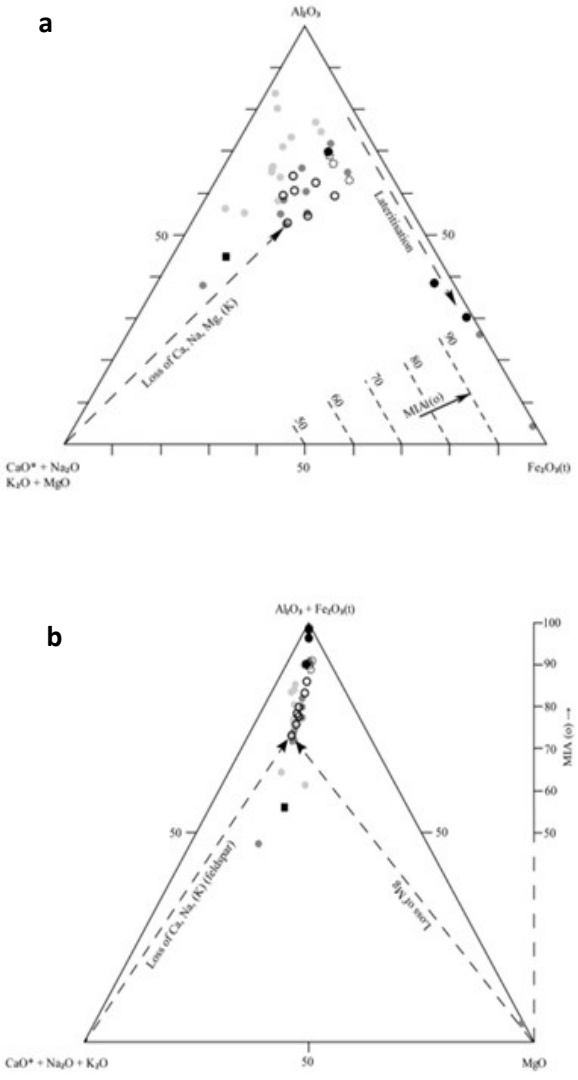

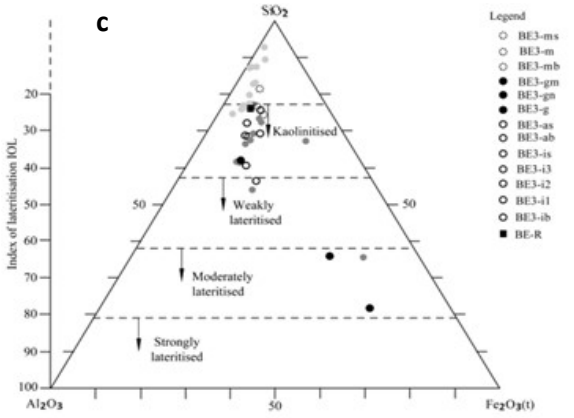

Fig. 6. (a) Molar Al_2O_3–CaO* + Na_2O + K_2O + MgO–$Fe_2O_{3(t)}$ (A–L–F), (b) Al_2O_3 + $Fe_2O_{3(t)}$–CaO* + NaO + K_2O–MgO (AF–CNK–M), and (c) mass SiO_2–Al_2O_3–$Fe_2O_{3(t)}$ (SAF) ternary plots illustrating the contribution of the mafic and felsic mineral components to rock weathering. Shaded circles are data from Kamgang et al. (2009) and Gong et al. (2011)

In the weathering profile of the Bengbis region, the values of IOL vary between 23 and 78. The studied materials are localised in the kaolinitisation domain (Fig. 6c). Only nodular materials undergo a moderate lateritisation. This fact is consistent with their position in the weathering profile. Fe^{2+}/Fe^{3+}ratios are relatively well-correlated with IOL (r^2 = 0.49). The transformation of Fe^{2+} into Fe^{3+}, in oxidised environment increases with the index of lateritisation.

Weathered materials are localised in the most resistant minerals domain (Fig. 7a). This fact seems counter-intuitive with the data of the SAF diagram which shows that kaolinitisation predominates in the studied weathering profile. However, it is justified by the abundance of quartz and goethite in these materials. Except for materials at the summit of the fine saprolite (hardpan), and that of the nodular horizon, kaolinitisation predominates in the Bengbis weathering materials (Fig. 7b).

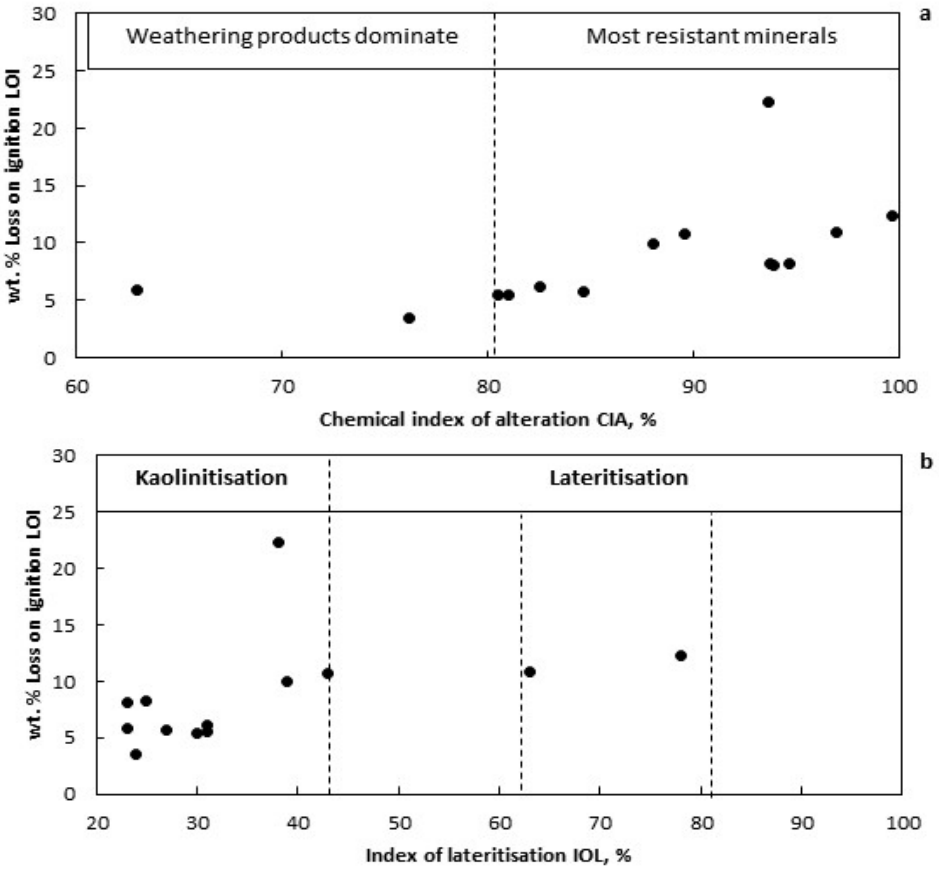

Fig. 7. Covariation of the loss on ignition (wt.%) with the (a) chemical index of alteration and (b) index of lateritisation

Several elements are regularly used as immobile elements to quantify gains and losses within weathered materials. Actually, Gresen's equation is applied to identify the immobile element (Chu et al., 2014) by calculating CIA values of all the samples and plotting graphically the chemical elements of the rock and that of the most weathered material in a cross plot. The isocon is U, W, Hf, Nb, Al_2O_3, and TiO_2. In the weathered materials of the Bengbis zone, the invariant element is hafnium (Fig. 8), which shows the lowest variations among all the other elements within the weathering profile in relation to the chlorite schists.

The geochemical mass balance calculations for the weathered materials are thus based on Hf as immobile element and the depletion or concentration factor is given by the following relationship (Brimhall and Dietrich, 1987; Anderson et al., 2002):

$$\tau_{j,w} = 100 \times [(C_{j,w}/C_{j,p})/(C_{Hf,w}/C_{Hf,p}) - 1] \quad (4)$$

In this model, the concentrations (C) of elements (j) in the parent rock (p), relative to that of an immobile index element (Hf), are used as a normalisation to establish the mass changes in the progressively altered rock (w). The combination of gains and losses of materials by mass balance calculations, chemical weathering indices present the advantage of linking high-precision trace elements to specific stages of weathering.

Very moderate losses in Si (< –18%) and average losses in Mg (–44 to –63%) associated with gains in Al and K in the coarse saprolite (Table 2) explain the presence of muscovite, sericite and interstratified illite/smectites. The lixiviation of K (–6%) in the fine saprolite justifies the disappearance of illite.

The presence of goethite and hematite is linked to the accumulation of Fe^{3+} in weathered materials. Fe^{3+} is perfectly linked to V ($r^2 = 1$) and strongly linked to Cu, Ga, Mo and Th ($r^2 = 0.81$) and Zr ($r^2 = 0.64$). These elements accumulate with the iron oxides and oxyhydroxides.

A relationship between the majority of alkali and alkaline earth elements (Li, Na, Rb, Mg, Ca, Sr, and Ba) is observed. Ca, Na and Sr are perfectly linked to the profile ($r^2 = 1$) and highly linked to Co ($r^2 = 0.81$). These elements, essentially contained in the plagioclases, are well-correlated with CIA and are quickly removed from the environment. Ca/Na ratio (0.28) of chlorite schists in Bengbis region is lower than that of Mbalmayo (Kamgang et al., 2009) which is 1.31. Bengbis rocks are less rich in plagioclases than

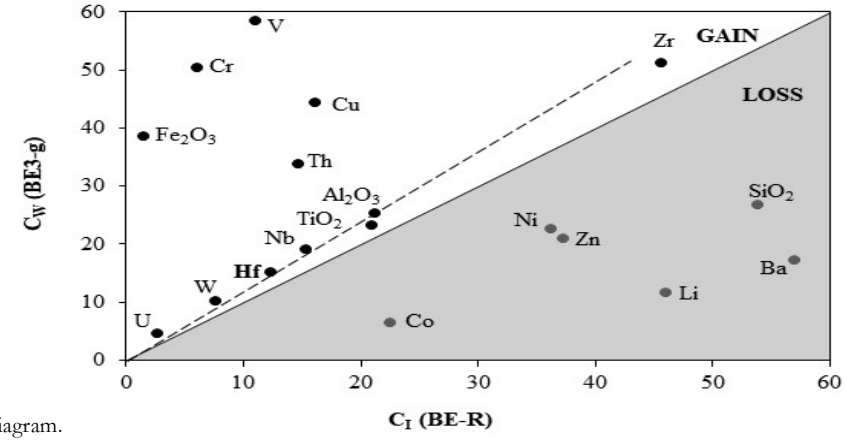

Figure 8. Isocon diagram.

Ci is the concentrations of the least weathered sample (BEr). Cw is the concentrations of the most weathered sample (BE3-g). The diagram is constructed for Fe_2O_3 in wt.%, SiO_2 in wt.%/1.2, Al_2O_3 in wt.% x 1.5, TiO_2 in wt.%/25, Nb, Ni, Th, U, and Li in ppm, Co in ppm/1.5, Cr in ppm/13, Hf in ppm x 2, V in ppm x 10, W in ppm x 5, Zn in ppm/2, Zr in ppm/5, Cu in ppm/1.8 and Ba in ppm/9. The isocon is U, W, Hf, Nb, Al_2O_3 and TiO_2.

Table 2. Geochemical mass balance calculations by isohafnium method of the Bengbis chlorite schist profile

	Parent rock	Saprolitic zone						Soil					
	Chlorite schist	Coarse saprolite					Fine saprolite		Nodular horizon			Sandy clayey horizon	
Code	BEr	BE3-ib	BE3-i1	BE3-i2	BE3-i3	BE3-is	BE3-ab	BE3-as	BE3-g	BE3-gn	BE3-gm	BE3-mb	BE3-m	BE3-ms
Si	*0.01*	0	-18	-12	-10	6	-30	-31	-53	-74	-15	24	16	26
Al	*0.01*	0	24	-26	26	28	27	42	33	13	-5	63	13	6	-13
Mg	*0.01*	0	-57	-63	-46	-52	-44	-57	-57	-85	-96	-69	-76	-77	-81
Mn	*0.01*	0	-50	-71	-65	-52	-58	-18	18	-64	-89	-71	-55	-59	-58
Ca	*0.01*	0	-97	-100	-99	-95	-100	-100	-96	-95	-100	-94	-97	-93	-97
Na	*0.01*	0	-97	-98	-98	-97	-98	-98	-98	-99	-100	-98	-100	-99	-99
K	*0.01*	0	28	16	65	38	71	-1	-6	-77	-90	-46	-66	-63	-71
Fe^{3+}	*0.01*	0	21	12	34	48	116	158	78	580	751	86	99	41	4
Fe^{2+}	*0.01*	0	-74	-94	-72	-79	-72	-88	-91	-100	-100	-92	-94	-90	-86
Ti	*0.01*	0	12	-7	8	24	28	13	22	6	-12	18	39	64	50
P	*0.01*	0	26	-80	-1	-40	57	24	-46	-45	-49	-63	-75	-60	-71
Rb	*0.23*	0	-59	-32	-48	2	-26	-64	1	-58	-85	-23	-33	-19	-35
Sr	*0.6*	0	-79	-89	-71	-86	-75	-96	-83	-91	-93	-85	-89	-86	-89
Ba	*0.8*	0	-37	-27	-27	6	13	-57	-15	-71	-83	-49	-70	-67	-75
Cs	*0.013*	0	2	18	41	46	51	18	43	-39	-78	39	9	11	-6
Li	*0.4*	0	-42	-46	-23	-20	-43	-37	-29	-76	-92	-43	-51	-51	-64
Nb	*0.028*	0	-2	-10	13	19	10	34	33	18	-3	56	39	45	32
Th	*0.06*	0	-13	-26	-19	-11	0	-48	-1	120	153	28	-2	-4	-22
U	*0.007*	0	53	9	45	53	130	90	8	64	79	27	5	3	-11
Zr	*4*	0	-2	-3	-5	-1	-4	-3	-2	7	14	3	-2	0	-1
W	*0.05*	0	6	8	47	33	36	65	35	26	12	43	8	8	-9
Mo	*0.08*	0	1588	454	1370	585	1457	1939	1389	5101	3287	1868	1492	1365	1124
Cr	*8*	0	-3	-7	22	30	15	77	73	683	823	30	47	25	-11
Ni	*0.8*	0	42	-66	-17	-22	1	57	-23	-41	-64	-4	-33	-34	-45
V	*1*	0	6	9	37	40	31	55	58	407	371	69	34	16	-8
Co	*0.1*	0	-48	-81	-68	-72	-63	-49	-55	-73	-75	-58	-59	-60	-64
Sc	*0.60*	0	-33	-16	-43	78	64	38	53	110	155	81	4	14	-20
Be	*0.04*	0	36	3	55	35	42	14	-12	-60	-69	-31	-56	-63	-68
Cu	*0.7*	0	65	-36	-5	-12	78	34	12	163	290	24	18	3	-14
Cd	*0.013*	0	-31	-30	-26	-35	-25	-16	-27	-6	-2	-14	-30	-6	-25
Ga	*0.04*	0	11	0	30	28	34	34	35	84	108	56	10	8	-15
Tl	*0.005*	0	619057	575995	680243	28	658285	695260	21	-51	558521	784681	853260	-10	913854
LREE	-	0	268	-62	172	-65	285	-79	-15	-60	-76	-32	-51	-42	-63
MREE	-	0	31	-74	100	-71	57	-56	-51	-75	-82	-65	-72	-65	-77
HREE	-	0	-18	-56	-1	-40	-8	-70	-47	-53	-53	-46	-53	-38	-51

those of Mbalmayo. Ca/Na ratios values are less constant in the weathering profile. The weathered materials where leaching of Ca compared with that of Na is greater and those where leaching of Na is more pronounced are observed. This fact is probably due to the predominance of Ca-feldspar or Na-feldspar in each of these materials. Magnesium is highly linked to Li ($r^2 = 0.81$) and Ba ($r^2 = 0.64$) and present tendencies of correlations with Rb ($r^2 = 0.47$). Lithium, Ba and Rb are perfectly correlated to Fe^{2+} ($r^2 = 1$). These elements are linked to the hydrolysis of mafic minerals. The leaching of Mg is less intense than that of Ca, Na and Fe^{2+} as illustrated by the evolution curves of CIA and MIA. The change in behaviour of Mg in the studied weathering environment is expressed by low values of the Ca/Mg ratio which varies between 0.00 and 0.11, as observed by Babechuk et al. (2014) for the weathered materials over basalts in India.

Potassium, Be and Cs remain in the alterites and are strongly linked (Table 2, Fig. 9). Beryllium and K are perfectly correlated in the alterites ($r^2 = 1$) and evacuated in the soils while Cs continues to accumulate. Potassium and Be are leached in the soils in association with Mg. The enrichments in K, Cs and Be in saprolites are linked to the presence of illite. The accumulation of Cs in the soil might be due to the presence of kaolinite in the weathered materials (Lim et al., 1980; Ugur and Sahan, 2012). High gains in Tl, up to 784 681%, in weathered materials are associated with the presence of Fe^{3+}, and consequently that of goethite and hematite in the weathering environment.

In general, a saw-toothed behaviour of all the elements can be observed along the studied profile (Fig. 9).

The constancy of the HFSE ratios (Fig. 10) suggests that they behaved more or less equally immobile, except for Th. But, the most stable system is: Hf – Nb – W – U.

4.3. REE fractionation

The concentrations of REE in the weathered materials as well as the characteristic ratios (ΣREE, LREE/HREE, $(La/Yb)_N$, Ce/Ce*, Eu/Eu*, Table 1) yield some remark insight into their behaviour.

LREE (La-Sm) are more abundant than other REE (Table 1). These elements present a saw-toothed evolution along the profile. Their contents range from 207 ppm in the chlorite schist to 814 ppm at the bottom of the coarse saprolite (BE3-ib). The coarse saprolite presents the highest contents in LREE. They are found in BE3-ib, BE3-i2 (566.54 ppm) and BE3-is (777.47 ppm) materials. The summit of the fine saprolite is around 4.5 times richer in LREE than its base. Nodules show low LREE contents (58.17 ppm) as compared to the matrix (138.74 ppm). These elements are mostly concentrated in the middle (BE3-m) of the loose clayey set (124.88 ppm). Cerium is the most abundant LREE. Its concentrations vary between 25.84 ppm (BE3-ab) and 441.00 ppm (BE3-ib).

MREE (Eu-Tb) are the less abundant REE. Their contents decrease from the chlorite schist (11.04 ppm) up to the bottom of the coarse saprolite (8.99 ppm). This fact is contrary to the increase observed for LREE in this set. The highest contents in MREE are observable at the bottom (8.99 ppm), in the medium horizon (17.48 ppm) and at the top (12.01 ppm) of the coarse saprolite. The base of the fine saprolite (1.78 ppm) is ~2.7 times more depleted in MREE than the summit (4.78 ppm). The matrix has slightly higher contents (2.78 ppm) than the ferruginous nodules. Loose clayey materials present low MREE contents (< 3 ppm). Gadolinium (1.38–12.08 ppm) and Tb (0.21–1.64 ppm) present the average

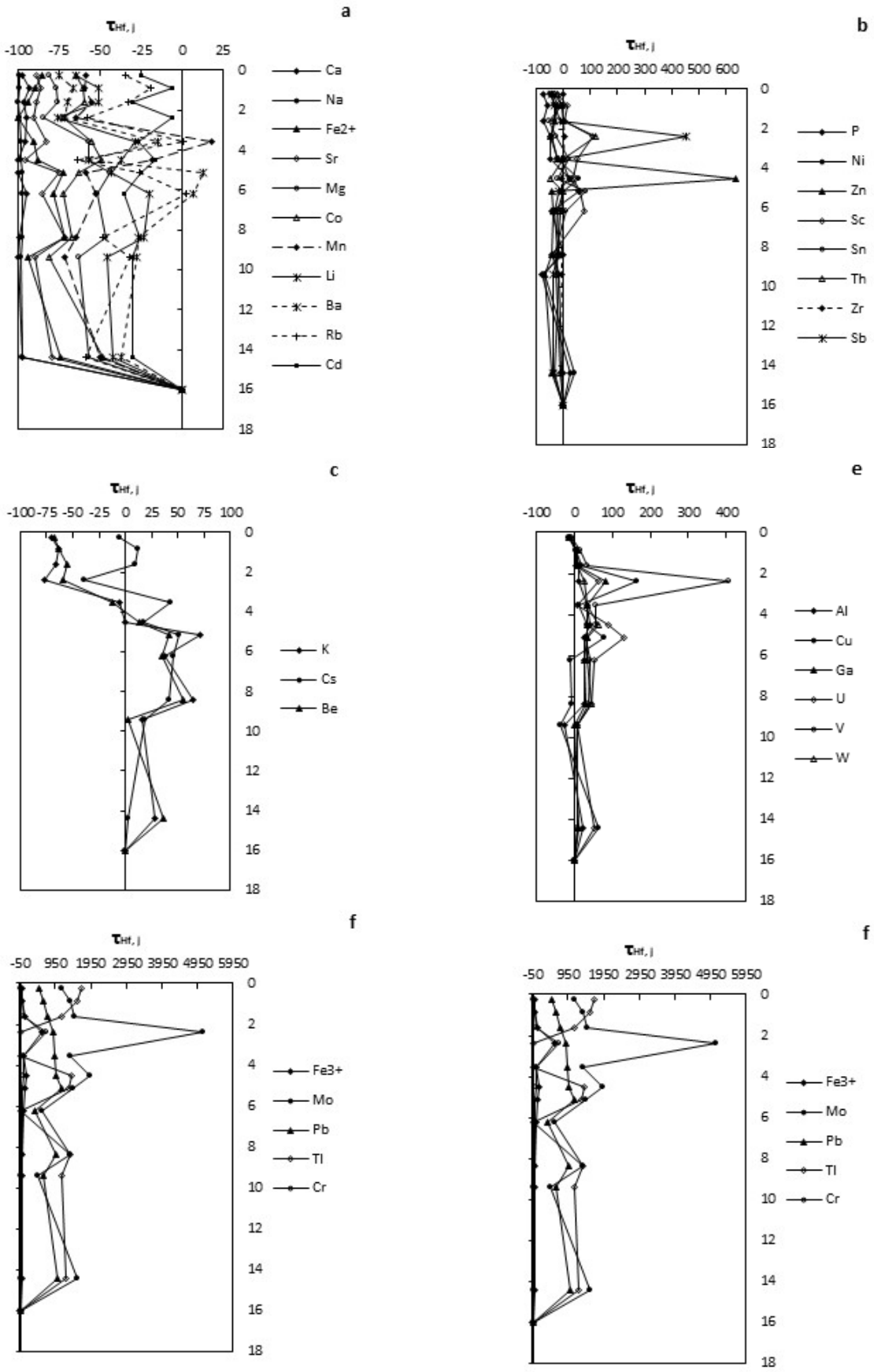

Fig. 9. Geochemical variation with constant Hf in the weathering profile

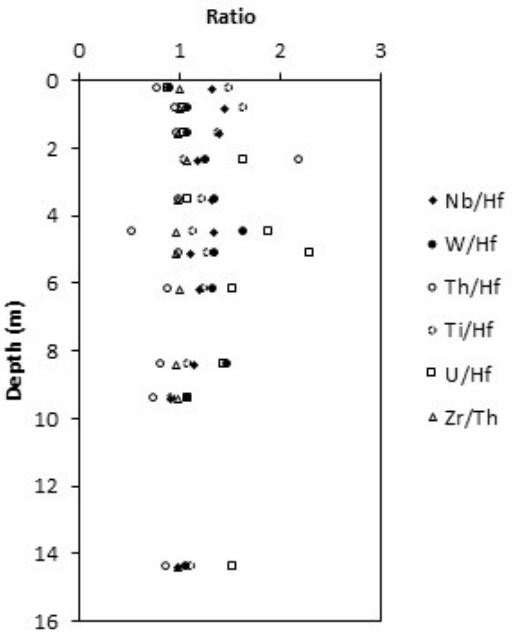

Fig. 10. HFSE elements ratios *vs.* depth in the profile

maximal and minimal contents of the weathering profile.

HREE (Dy-Lu) contents are intermediate between those in LREE and MREE. HREE also presents a saw-toothed general evolution along the profile. Their contents at the bottom of the coarse saprolite (11.17 ppm) decrease of ~23% compared with those of the chlorite schist (14.41 ppm). The highest content in HREE (15.52 ppm) is that of the medium facies of the coarse saprolite. These contents are comparable at the bottom (11.17 ppm) and at the top (11.69 ppm) of this level. The summit of the fine saprolite (8.29 ppm) is ~ 2 times enriched in HREE than its base (4.18 ppm). As opposed to the LREE and MREE, ferruginous nodules are relatively more enriched in HREE than the matrix. In the loose clayey set, the distribution of HREE is like that of other REE. The medium part of this set presents the highest content (7.62 ppm). The contents of clayey materials of the base and of the summit of this set do not exceed 6.00 ppm.

Some materials of the coarse saprolite of the Bengbis weathering profile are depleted in REE in relation to chlorite schists, according to the order HREE > MREE > LREE. This order of mobility of REE is well known and consistent with the works of many authors (Braun et al., 1993; Laveuf and Cornu, 2009; Gong et al., 2011; Babechuk et al., 2014; Sababa et al., 2015) which showed that HREE are more mobile than LREE during the weathering process. The mobility of HREE and LREE is comparable in the coarse saprolite, fine saprolite, nodular level and loose clayey materials depleted in REE according to the order MREE > HREE ~ LREE (Fig. 11). This fact is counter-intuitive, because HREE are more mobile in supergene environment than the LREE. Kamgang et al. (2009) report higher mobility of LREE compared with HREE in the weathered materials on chlorite schists in the Mbalmayo region. This phenomenon can be because the Bengbis materials are acidic (4.78 < pH < 5.75) and those of Mbalmayo, weakly acidic to basic (6.70 < pH < 7.80).

In the Bengbis region, LREE and MREE accumulate in the coarse saprolite for pH values comprised between 5.5 and 5.6 and for those of Eh varying between +60 and +70mV. Contrary to the work of Gong et al. (2013), LREE are not adsorbed by clays during pedogenesis, despite the abundant presence of kaolinite in the loose clayey materials. Adsorption or co-precipitation of LREE onto Fe oxides mainly may control the concentration of these elements in this part of the profile (Ren et al., 2015). $(La/Yb)_N$ values are very close to 1 in almost all the materials of the profile except for some materials of the saprolite, thus showing a slight fractionation between LREE and HREE.

The fractionation between neighbouring REE is not detectable (Sm/Nd ~1), except for the basal coarse saprolite, where Sm/Nd ratio is equal to 0.76. In fact, this material has the highest content in Ce (441.00 ppm). This is the same for materials

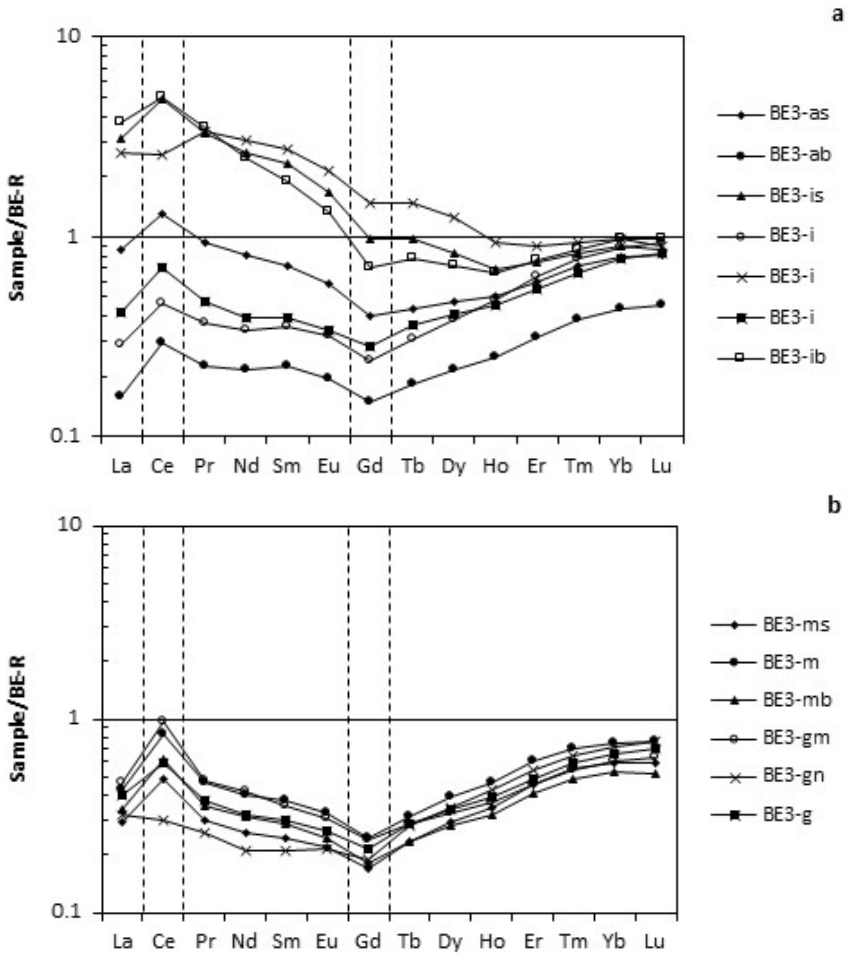

Fig. 11. Chlorite schist-normalized REE plots for (a) saprolites and (b) soils of the Bengbis profile

of the Mbalmayo area (Kamgang et al., 2009), where the fractionation between neighboring REE was only observed in the basal coarse saprolite. This well-known fact (Ndjigui et al., 2008; Kamgang et al., 2009; Wang et al., 2013) is due to the accumulation of REE and mostly of Ce at the base of the lateritic weathering profiles. The parent rock constitutes by its nature and its pH, a barrier to the vertical migration of these elements.

Weathered materials do not present anomalies for values ranging between 0.90 and 1.10 (Braun et al., 1993). The values of the Eu/Eu* ratio range between 1.02 and 1.15. Weathered materials in the Bengbis area do not present anomalies in europium. The absence of anomalies in europium Eu/Eu* indicates complete dissolution of feldspar in the weathered materials.

The parent rock has a negative Ce anomaly. This is not expected for an unweathered rock. This creates three issues with the internal normalization strategy (1) negative Ce anomalies in the rest of the weathering profile can be masked, (2) any existing positive Ce anomaly is amplified, and (3) positive Ce anomalies can appear where there are none. In fact, in hot and humid tropical areas, it is difficult to collect an 'unweathered' rock, except when you have fresh road cuttings. Ce/Ce* values vary between 0.87 and 2.06. The median coarse saprolite facies presents very low negative cerium anomaly (Ce/Ce* = 0.87). All other parts of the studied profile show mild positive anomalies (Ce/Ce* ~1.17 – 1.58). REE patterns with positive cerium anomaly and enriched in LREE compare to HREE correspond to saprolitic materials. In all other parts of the profile, materials present

weak positive Ce anomalies but are depleted in REE. Positive anomalies in Ce are a well-known fact in supergene alterations (Braun et al. 1993; Ndjigui et al. 2008; Kamgang et al. 2009; Ren et al., 2015; Sababa et al. 2015; Onana et al., 2016). They are due to the change in Ce^{3+} to Ce^{4+}. The weak positive anomalies in Ce, despite the degree of weathering of materials in the Bengbis area, are probably due to the presence of low amounts of rhabdophane as indicated by correlations between Ce – P_2O_5 ($r^2 = 0.49$), Ce – La ($r^2 = 1$) and Ce – Nd ($r^2 = 0.81$) as well as the low content in P_2O_5 (< 0.25 wt. %) in the weathering environment.

The values of Gd/Gd* vary between 0.70 and 0.84. Weathered materials of the Bengbis area present Gd fractionation. This fractionation materialises the similitude of behaviour between LREE and HREE and the MREE depletion. These values of Gd/Gd* corroborate the data of $(La/Yb)_N$. Gadolinium is linked to Fe^{2+}, Mg, Li and Ni which are highly leached elements of this environment ($r^2_{(Fe^{2+}, Mg, Li, Ni) - Gd} = 0.40$). Gadolinium is thus present in mafic minerals. This element which does not have the possibility to change its valence to remain stable in the weathering milieu, is leached, hence a negative anomaly is observed. It appears that, a part of Gd distribution and remobilization is controlled by mafic minerals in the studied weathered materials. Gadolinium fractionation is thus due to intense chemical leaching.

5. Conclusions

This work investigates the intensity of weathering, and elements (alkali and alkaline earth elements and REE) released in a lateritic profile overlying chlorite schists from Bengbis in the southern Cameroon. The main conclusions are as follows:

(1) The hydrolysis of the feldspars (losses in Ca, Na and K) is proportional to that of the mafic minerals (loss in Mg), although the dissolution of plagioclases is more intense than that of mafic minerals. The studied materials are localised in the kaolinitisation domain, except for the nodular materials which are slightly lateritised;

(2) The order of mobility of elements in the weathering environment is: Ca ≈ Na > Fe^{2+} .≈Sr > Mg Co > Mn > Li > Ba > Rb > P > Cd > Ni > Si > Be > K > Sn. The elements Ca, Na and Sr, essentially contained in the plagioclases are well-correlated to CIA and MIA. The change in behaviour of Mg in the weathering profile is expressed by low values of Ca/Mg ratio. Potassium and Be are leached in the soils in association with Mg. Enrichments in K, Cs and Be in saprolites are linked to the presence of illite. The accumulation of Cs in the soils is due to the presence of kaolinite;

(3) REE exhibit three types of behaviour along the Bengbis profile as indicated by the $(La/Yb)_N$ ratio values which are less than 1, higher than 1 and ~1. REE are not adsorbed by clays during the pedogenesis, despite the abundance of kaolinite in the loose sandy clayey materials. Weak Ce anomalies, despite the degree of weathering are probably due to the presence of low amounts of rhabdophane. The weathered materials of the Bengbis area present a fractionation in Gd.

Acknowledgments

The authors express their gratitude to the GeoLabs (Sudbury-Canada) for mineralogical and chemical analyses. They also express their gratitude to anonymous reviewers who improved considerably the manuscript.

References

Anderson, S.P., Dietrich, W.E., Brimhall Jr., G.H. (2002). Weathering profiles, mass-balance analysis, and rates of solute loss: linkages between weathering and erosion. Geology Society American Bulletin 114, 1143–1158.

Babechuk, M.G., Widdowson, M., Kamber, B.S. (2014). Quantifying chemical weathering intensity and trace element release from two contrasting basalt profiles, Deccan Traps, India. Chemical Geology 363, 56–75.

Bao, Z., Zhao, Z. (2008). Geochemistry of mineralization with exchangeable REY in the weathering crusts of granitic rocks in South China. Ore Geology Reviews 33, 519–535.

Bitom, D. and Volkoff, B. (1993). Altération déferruginisante des cuirasses massives et formation des horizons gravillonnaires ferrugineux dans les sols de l'Afrique Centrale humide. Comptes Rendus de l'Académie des Sciences II, 1447–1454.

Bourdon, B., Bureau, S., Andersen, M.B., Pili, E., Hubert, A. (2009). Weathering rates from top to bottom in a carbonate environment. Chemical Geology 258, 275–287.

Braun J.J. (1991). Comportement géochimique et minéralogique des Terres Rares, du thorium et de l'uranium dans le profil latéritique d'Akongo (Sud-Ouest Cameroun). Thèse Doct. Univ. Nancy, France, 236 p.

Braun, J.J., Pagel, M., Herbillon, A., Rosin, C. (1993). Mobilization and redistribution of REE and Th in syenitic lateritic profile: a mass balance study. Geochimica and Cosmochimica Acta 57, 4419–4434.

Brimhall, G.H., Dietrich, W.E. (1987). Constitutive mass-balance relations between chemical composition, volume, density, porosity and strain in metasomatic hydrochemical systems: results on weathering and pedogenesis. Geochimica and Cosmochimica Acta 57, 4419–4434.

Chu, H., Chi, G., Bosman, S., Card, C. (2014). Diagenetic and geochemical studies of sandstones from drill core DV10-001 in the Athabasca basin, Canada, and implications for uranium mineralization. Journal of Geochemical Exploration 148, 206–230.

Duchaufour, P. (1977). Pédogénèse et classification. Masson Ed., (France), 477 p.

Fedo, C.M., Nesbitt, H.W., Young, G.M. (1995). Unravelling the effects of potassium metasomatism in sedimentary rocks and paleosols, with implications for paleoweathering conditions and provenance. Geology 23, 921–924.

Flint, L.E., Flint, A.L. (2002). Methods of Soil Analysis, Part 4, Physical Methods: Porosity. Soil Science Society of America Book Series Ed., 241–254.

Gardner, R., Walsh, N. (1996). Chemical weathering of metamorphic rocks from low elevations in the southern Himalaya. Chemical Geology 258, 275–287.

Gong Q., Deng J., Yang L., Zhang J., Wang Q., Zhang G. (2011). Behaviour of major and trace elements during weathering of sericite-quartz schist. Journal of Asian Earth Sciences 42, 1–13.

Gromet L.P., Dymek R.F., Haskin L.A. et Korotev R.L. (1984). The 'North American Shale Composite'. its compilation, majors and trace

elements characteristics. Geochimica and Cosmochimica Acta, 48, 2469–2482.
Irfan, T.Y. (1999). Characterization of weathered volcanic rocks in Hong Kong. Quarterly Journal of Engineering Geology 32, 31–34.

Kamgang Beyala, V. (1987). Altération supergène des roches grenatifères de la région de Yaoundé (Cameroun): Pétrologie, Minéralogie. Th. Doct. 3ème cycle, Univ. Poitiers, 170 p.

Kamgang Kabeyene Beyala, V., Onana, V.L., Ndome Effoudou Priso, E., Parisot, J.C., Ekodeck, G.E. (2009). Behavior of REE and mass balance calculations in a lateritic profile over chlorite schists in South Cameroon. Chemie Der Erde-Geochemistry 69, 61–73.

Laveuf, C., Cornu, S. (2009). A review on the potentiality of Rare Earth Elements to trace pedogenetic processes. Geoderma 154, 1–12.

Lim, C.H., Jackson, M.L., Koons, R.D., Helmke, P.A. (1980). Kaolins: sources of differences in cation-exchange capacities and cesium retention. Clays and clay minerals 28(3), 223–229.

Munsell Color (2000). Charts. Macbeth Division of Kollmorge Corporation, 2441 North Calvert Street Baltimore, Maryland 21218.

Ndjigui, P.-D., Bilong, P., Bitom, D., Dia, A. (2008). Mobilization and redistribution of major and trace elements in two weathering profiles developed on serpertinites in the Lomie´ ultramafic complex, South-East Cameroon. Journal of Asian Earth Sciences 42, 1–13.

Nesbitt, H.W. (1992). Diagenesis and metasomatism of weathering profiles, with emphasis on Precambrian paleosols. In: Martini, I.P., Chesworth, W. (Eds.), Weathering, Soils & Paleosols. Elsevier, Netherlands, pp. 4.1.

Nesbitt, H.W., Markovics, G. (1997). Weathering of granodiorite crust, long-term storage of elements in weathering profiles, and petrogenesis of siliclastic sediments. Geochemica et Cosmochica Acta 61, 1653–1670.

Nesbitt, H.W., Wilson, R.E. (1992). Recent chemical weathering of basalts. American Journal of Science 292, 740–777.

Nesbitt, H.W., Young, G.M. (1982). Early Proterozoic climates and plate motions inferred from major element chemistry of lutites. Nature 299, 715–717.

Nesbitt, H.W., Young, G.M. (1982). Prediction of some weathering trends of plutonic and volcanic rocks based on thermodynamic and kinetic considerations. Geochimica and Cosmochimica Acta 57, 4419–4434.

Nesbitt, H.W., Young, G.M. (1982). Formation and diagenesis of weathering profiles. Journal of Geology 97, 129–147.

Nesbitt, H.W, Young, G.M. (1984). Prediction of some weathering trends of plutonic and volcanic-rocks based on thermodynamic and kinetic considerations. Geochimica et Cosmochimica Acta 48(7),1523–1534.

Nguetnkam, J.P., Yongue-Fouateu, R., Bitom, D., Volkoff, B. (2006). Etude pétrologique d'une formation latéritique sur granite en milieu tropical forestier sud-camerounais (Afrique centrale), mise en évidence de son caractère polyphasé. Etude et Gestion des sols 13(2), 89–102.

Numbem Tchakounté J., Toteu, S.F., Van Schmus, W. R., Penaye, J., Deloule, E., Mvondo Ondoa, J., Bouyo Houketchang, M., Ganwa, A. A., White, W. M. (2007). Evidence of ca 1.6-Ga detrital Zircon in the Bafia Group (Cameroon): Implications for the chronostratigraphy of the Pan-African Belt Nord of the Congo Craton. Comptes Rendus Géosciences 339(2), 132–142.

Nyassa Ohandja, H., Onana, V.L., Noa Tang, S.D., Ngo'o Ze, A., Ekodeck, G.E. (2020). Behavior of major, trace, and rare earth elements in an atypical lateritic profile overlying micaceous quartzites, Centre Cameroon: imprint of the parent rock structure. Arabian Journal of Geosciences 13, 869.

Onana V.L. (2010). Altération supergène des chloritoschistes de la série de Mbalmayo-Bengbis et implications géotechniques. Th. Doct./Ph. D, Fac. Sci. Univ. Yaoundé I, 246 p.

Onana V.L., Ntouala R.F.D., Noa Tang S.D., Ndome Effoudou E., Kamgang Kabeyene V., Ekodeck G.E. (2016). Major, trace and REE geochemistry in contrasted chlorite schist weathering profiles from southern Cameroon: Influence of the Nyong and Dja Rivers water table fluctuations in geochemical evolution processes. Journal of African Earth Sciences 124: 371–382.

Owona, S., Schulz, B., Ratschbacher L., Mvondo Ondoa, J., Ekodeck, G.E., Tchoua, M.F. Affaton, P. (2010). Pan-African metamorphic evolution in the southern Yaounde Group (Oubanguide Complex, Cameroon) as revealed by EMP-monazite dating and thermobarometry of garnet metapelites. Journal of African Earth Sciences 59(1): 125–139.

Patino, L.C., Velbel, M.A., Price, J.R., Wade, J.A. (2003). Trace element mobility during spheroidal weathering of basalts and andesites in Hawaii and Guatemala. Chemical Geology 258, 275–287.

Rajamani, V., Tripathi, J.K., Malviya, V.P. (2009). Weathering of lower crustal rocks in the Kaveri river catchment, southern India: implications to sediment geochemistry. Chemical Geology 258, 275–287.

Ren, L., Cohen, D.R., Rutherford, N. F., Zissimos, A., M., Morisseau, E.G. (2015). Reflections of the geological characteristics of Cyprus in soil rare earth element patterns. Applied Geochemistry 56, 80–93.

Sababa E., Ndjigui, P.-D., EbahAbeng S., Bilong, P. (2015). Geochemistry of peridotite xenoliths from the Kumba and Nyos areas (southern part of the Cameroon Volcanic Line): Implications for Au–PGE exploration. Journal of Geochemical Exploration 148, 206–230.

Santoir C. (1995). Atlas régional du Sud Cameroun. Vol. Oro - hydrographie, ORSTOM éd., 4–5.

Smith, D.B, (1998). United States Geological Survey - Certificate of Analysis. Mica schist SDC-1. 1–3.

Suchel, J.B., Tsalefac, M. (1995). Atlas régional du Sud Cameroun. Vol. Climatologie, ORSTOM éd., 8–9.

Tardy, Y. (1993). Pétrologie des latérites et des sols tropicaux. Masson Ed. (France), 461 p.
Ugur, F.A., Sahan, H. (2012). Sorption behaviour of ^{137}Cs on kaolinite. Ekoloji 21, 82, 34–40. doi: 10.5053/ekoloji.2011.825

Walter, A.-V., Nahon, D., Flicoteaux, R., Girard, J.P., Melfi, A. (1995). Behaviour of major and trace elements and fractionation of REE under tropical weathering of a typical apatite-rich carbonatite from Brazil. Earth and Planetary Science Letters 136, 591–602.

Wang, X., Jiao, Y., Du, Y., Ling, W., Wu, L., Cui, T., Zhou, Q., Jin, Z., Lei, Z., Weng, S. (2013). REE mobility and Ce anomaly in bauxite deposit of WZD area, Northern Guizhou, China. Journal of Geochemical Exploration 148, 206–230.

Zheng, Z., Lin, C. (1996). The behavior of Rare-Earth elements (REE) during weathering of granites in Southern Guangxi, China. Chinese Journal of Geochemistry 15, 344–352.